Contribution from the Department of Chemistry,
University of Houston, Houston, Texas 77204-5641

Synthesis and Molecular Structure of $Rh_2(ap)_4(CCH)$ (ap = 2-Anilinopyridinate). Spectroscopic and Electrochemical Properties of Carbon-σ-Bonded Dirhodium Complexes

C.-L. Yao, K. H. Park, A. R. Khokhar,† M.-J. Jun,‡ and J. L. Bear*

Received March 14, 1990

The reactions of tetrakis(μ-2-anilinopyridinato)dirhodium(II,III) chloride, $Rh_2(ap)_4Cl$, with NaR or LiR, where R is the terminal acetylide ion (C≡CH, C≡CC_6H_5, C≡CC_5H_{11}, or C≡CC_4H_8C≡CH), results in the nucleophilic substitution of the axial chloride with the aliphatic group to form a Rh–C σ bond. The complex $Rh_2(ap)_4(C{\equiv}CH)$, $C_{46}H_{37}N_8Rh_2{\cdot}CH_2Cl_2$, crystallizes in the triclinic space group $P\bar{1}$ with two formula weights in a unit cell having dimensions a = 10.970 (3) Å, b = 13.343 (3) Å, c = 14.445 (3) Å, α = 87.22 (2)°, β = 87.60 (2)° and γ = 83.13 (2)° and refined to $R(F_o)$ = 0.039. The Rh–Rh bond distance is 2.439 Å. $Rh_2(ap)_4(R)$ complexes are also characterized by ESR, mass, IR, and UV–vis spectra. The Rh–C-bonded complexes and the axially uncoordinated radical cation $[Rh_2(ap)_4]^+$ all give axial ESR signals with $g_\parallel$ split into a doublet. Electrochemical studies show that both reduction and oxidation half-wave potentials of $Rh_2(ap)_4(R)$ are cathodically shifted from the potentials of their parent complex $Rh_2(ap)_4Cl$ and there is a second oxidation occurring around +1.0 V. In the presence of O_2, a new ESR signal corresponding to a bound superoxide ion is observed at 123 K, indicating formation of $Rh_2(ap)_4(R)(O_2)$.

Introduction

We recently reported the synthesis and characterization of two geometric isomers of $Rh_2(ap)_4$, where ap = 2-anilinopyridinate ion (a).[1,2] The 2,2-trans isomer (b) had two pyridyl nitrogen (N_p) and two anilino nitrogen (N_a) donor atoms of the bridging anilinopyridinate ions bound to each rhodium ion in a trans fashion. The 4,0 isomer (c) had four pyridyl nitrogens bound to one

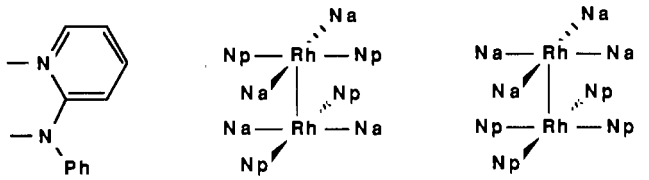

(a) (b) (c)

rhodium and four anilino nitrogens bound to the second rhodium. A large isomer effect was observed in the chemical and electrochemical reactivity of the two complexes, as well as in their electronic structures.[2] The most striking difference in the properties of the two geometric isomers was the distribution of spin density over the two metal centers of the radical cations. An axial ESR signal was observed for the 4,0 isomer with $g_\parallel$ split into a doublet, indicating that the odd electron is localized on one rhodium ion (^{103}Rh, $I = {}^1/_2$).[1,2] This degree of polarization of a metal-centered singly occupied molecular orbital (SOMO) had never been observed before for metal–metal-bonded mixed-valent complexes. A rhombic ESR signal was observed for the singly oxidized 2,2-trans isomer, and g_z appeared as a doublet of doublets with one axial ligand and a 1:2:1 triplet with none or two axial ligands.[1,2] Therefore the SOMO of this complex was equally distributed over both metal centers if the ligand interaction at the two axial sites was the same and polarized if different.

ESR results similar to those observed for the 2,2-trans isomer have been reported for the equatorially symmetric tetrakis(*N*,*N*′-diphenylbenzamidinato)dirhodium[3] and tetrakis(*N*,*N*′-ditolylformamidinato)dirhodium[4] complexes. The formation of one axial ligand bond clearly plays a significant role in the polarization of the SOMO. However, there are three factors that could cause the spin localization observed for the 4,0 isomer $[Rh_2(ap)_4]^+$. These are (1) the difference in the equatorial ligand fields of two rhodium ions, (2) the torsion angle of the equatorial rhodium planes, and (3) the formation of only one axial ligand bond. There are questions regarding the relative importance of these factors in the localization of the SOMO as well as which rhodium ion contains the odd electron in the presence and absence of an axial ligand.

The 4,0 isomer of $[Rh_2(ap)_4]^{0/+}$ in the presence of nonbonding anions such as ClO_4^- or strong σ donors such as alkyl anions should provide unique Rh^{II}_2, $Rh^{II}Rh^{III}$, and Rh^{III}_2 dimetal complexes for investigating the relative importance of axial vs equatorial ligand polarization of the HOMO or SOMO. In this regard, we report the synthesis and molecular structure $Rh_2(ap)_4(C{\equiv}CH)$. The ESR spectra and electrochemical properties of $[Rh_2(ap)_4(L)]^{n+}$ ($Rh_2(ap)_4$ = the 4,0 isomer; n = 0, 1, 2; L = ClO_4^- or acetylide ion) are also reported. These rhodium–carbon σ-bonded complexes are the first reported dirhodium compounds containing an axial Rh–C bond other than CO complexes and one isocyanide complex[5] found in the literature.

Experimental Section

Chemicals. The 4,0 geometric isomer of $Rh_2(ap)_4Cl$ was prepared by a previously described procedure.[1,2] Tetrahydrofuran (THF) and CH_2Cl_2 were distilled over CaH_2 under Ar. Tetra-*n*-butylammonium perchlorate (TBAP) was obtained from Fluka Chemical Co., recrystallized twice from ethanol, and used as the supporting electrolyte for electrochemical measurements. Organolithium reagents were prepared by the reaction of the desired 1-alkynes with *n*-butyllithium in THF under Ar and used without further treatment. HC≡CNa (Aldrich) was obtained as suspensions in ether and used directly.

Synthesis of $Rh_2(ap)_4(R)$. $Rh_2(ap)_4(R)$ complexes were prepared by direct reaction of $Rh_2(ap)_4Cl$ with the desired organolithium reagents in a 1:5 molar ratio in dry THF at room temperature under Ar. The reaction was allowed to proceed for 30 min, during which time the color of the solution changed from purple red to reddish brown while a steady flow of Ar was maintained. The solvent was then removed by using a rotary evaporator, and the complex was twice purified on a silica gel column with CH_2Cl_2 as the eluent under air. Complexes were then recrystallized from CH_2Cl_2/hexane.

Purified $Rh_2(ap)_4(C{\equiv}CH)$ was further dried in a vacuum oven at 50 °C for 2 days, and the duplicate elemental analyses were performed by Texas Analytic Laboratories, Inc. Anal. Calcd. for $C_{46}H_{37}N_8Rh_2$: C, 60.87; H, 4.11; N, 12.34; Rh, 22.67. Found: C, 60.80; H, 4.08; N, 12.30; Rh, 22.59.

Large clusters of fused crystals of $Rh_2(ap)_4(C{\equiv}CH)$ were obtained by slow diffusion of hexane into a solution made up of a 20:1 ratio of CH_2Cl_2:CH_3OH and used for structural determination. Both crystals and powder forms of the sample were used in electrochemical and spectroscopic studies, and they showed no detectable differences. Attempts to grow crystals of other $Rh_2(ap)_4(R)$ complexes were not successful.

Instrumentation. Cyclic voltammetric measurements were carried out on an IBM Model 225 voltammetric analyzer by utilizing a three-elec-

† Present address: University of Texas M. D. Anderson Cancer Center.
‡ Present address: Yonsei University, Seoul, Korea.

(1) Bear, J. L.; Liu, L.-M.; Kadish, K. M. *Inorg. Chem.* **1987**, *26*, 2927.
(2) Bear, J. L.; Yao, C.-L.; Capdevielle, F. J.; Korp, J. D.; Albright, T. A.; Kang, S.-K.; Kadish, K. M. *Inorg. Chem.* **1989**, *28*, 1254.
(3) Le, J. C.; Chavan, M. Y.; Bear, J. L.; Kadish, K. M. *J. Am. Chem. Soc.* **1985**, *107*, 7195.
(4) Piraino, P.; Bruno, G.; Lo Schaivo, S.; Laschi, F.; Zanello, P. *Inorg. Chem.* **1987**, *26*, 2205.
(5) Girolami, G. S.; Andersen, R. A. *Inorg. Chem.* **1981**, *20*, 2040.

0020-1669/90/1329-4033$02.50/0

Table I. Data Collection and Processing Parameters

space group	$P\bar{1}$, triclinic	formula	$C_{46}H_{37}N_8Rh_2 \cdot CH_2Cl_2$
cell consts		fw	992.66
a, Å	10.970 (3)	Z	2
b, Å	13.343 (3)	ρ, g/cm^3	1.57
c, Å	14.445 (3)	μ, cm^{-1}	9.47
α, deg	87.22 (2)	λ, Å	0.71073
β, deg	87.60 (2)	$R(F_o)$	0.039
γ, deg	83.13 (2)	$R_w(F_o)$	0.038
V, Å^3	2095		

trode electrochemical cell. The working electrode was a platinum button with a surface area of 0.19 mm^2, and the potential reference was a saturated calomel electrode (SCE). Controlled-potential electrolysis was done on a BAS Model SP-2 synthetic potentiostat. ESR spectra were measured on an IBM Model 100D spectrometer. Mass spectra were obtained on a VG Analytical 70-SEQ mass spectrometer by using the fast atom bombardment (FAB) method. UV–visible spectra were recorded on a Perkin-Elmer 330 spectrophotometer with a 1.0 cm path length cell, and IR spectra were recorded on an IBM Model IR/32 FTIR spectrometer.

X-ray Crystallography

A small, blackish purple slab, having approximate dimensions 0.24 × 0.22 × 0.12 mm, was cut from the stem of a very large cluster of fused crystals. The crystal was then mounted on a glass fiber in a random orientation on a Nicolet R3m/V automatic diffractometer. The radiation used was Mo Kα monochromatized by a highly ordered graphite crystal. Final cell constants, as well as other information pertinent to data collection and refinement, are listed on Table I. The Laue symmetry was determined to be $\bar{1}$, and the space group was shown to be $P\bar{1}$. Intensities were measured by using the ω-scan technique, with the scan rate depending on the count obtained in rapid prescans of each reflection. Two standard reflections were monitored after every 2 h or every 100 data collected, and these showed an isotropic, linear decay of 16% during the 4 days of data collection. A normalizing factor as a function of exposure time was included in order to account for this. In reduction of the data, Lorentz and polarization corrections were applied; however no correction for absorption was made due to the small absorption coefficient.

The structure was solved by interpretation of the Patterson map, which yielded the positions of the two Rh atoms in the asymmetric unit. The remaining non-hydrogen atoms were located in subsequent Fourier syntheses. The usual sequence of isotropic and anisotropic refinement was followed, after which all hydrogens were entered in ideal calculated positions and constrained to riding motion, with a single variable isotropic temperature factor for all of them. The acetylenic hydrogen was held fixed. A molecule of methylene chloride solvent was also located and was found to refine best with use of a population factor of 75%. Presumably, loss of this solvent was the cause of the aforementioned intensity decay. On the assumption that some solvent was already lost prior to the commencement of data collection, all quantities in Table I were calculated on the basis of 100% solvent occupancy. After all shift/esd ratios were less than 1.0, convergence was reached at the agreement factors listed in Table I. No unusually high correlations were noted between any of the variables in the last cycle of full-matrix least-squares refinement, and the final difference density map showed a maximum peak of about 0.6 e/Å^3. All calculations were made with the Nicolet SHELXTL PLUS (1987) series of crystallographic programs.

Results

$Rh_2(ap)_4(C{\equiv}CH)$ was characterized by X-ray crystallography, and its structural view is given in Figure 1. The atomic coordinates of the key atoms for this complex are listed in Table II. The selected bond lengths and angles are contained in Table III. For comparison, Table IV lists selected average bond lengths and

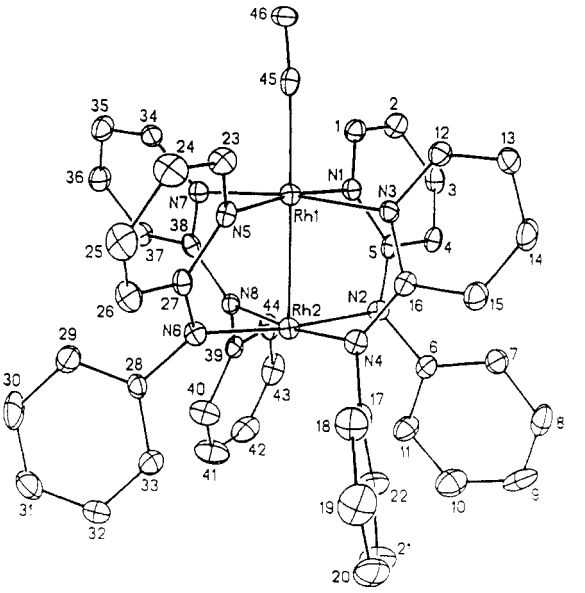

Figure 1. Labeled ORTEP diagram of $Rh_2(ap)_4(C{\equiv}CH)$.

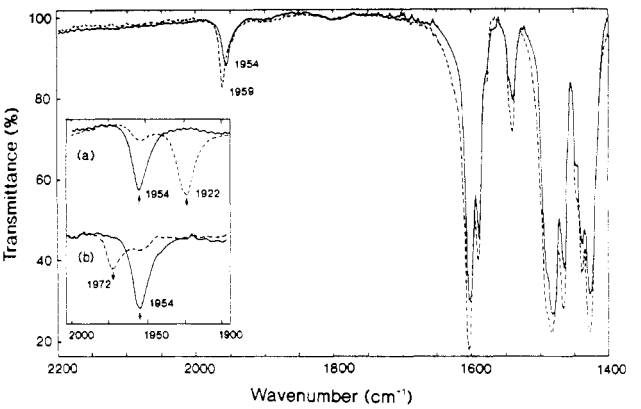

Figure 2. IR spectra of $Rh_2(ap)_4(C{\equiv}CH)$ after evaporating CH_2Cl_2 solution under N_2 (solid line) and O_2 (dashed line). Insets: (a) neutral (—) and singly reduced (- -) $Rh_2(ap)_4(C{\equiv}CH)$; (b) neutral (—) and singly oxidized (- -) $Rh_2(ap)_4(C{\equiv}CH)$, in CH_2Cl_2, 0.1 M TBAP.

bond angles for $Rh_2(ap)_4(C{\equiv}CH)$ and its parent complex, $Rh_2(ap)_4Cl$.

The complexes were characterized by mass spectrometry and infrared spectroscopy. The mass spectrum (see supplementary material) of $Rh_2(ap)_4(C{\equiv}CC_6H_5)$ shows the molecular ion peak at m/e = 983, corresponding to $[Rh_2(ap)_4(C{\equiv}CC_6H_5)]^+$, while the molecular ion $[Rh_2(ap)_4]^+$ is found at m/e = 882. The mass spectrum of $Rh_2(ap)_4(C{\equiv}CC_5H_{11})$ shows the molecular ion peak m/e = 977. The peak at m/e = 882 for the complex is again due to $[Rh_2(ap)_4]^+$, while the peak observed at m/e = 995 is probably due to the hydrated form of the molecular ion, $[Rh_2(ap)_4(C{\equiv}CC_5H_{11})(H_2O)]^+$. The mass peak at m/e = 1047 is consistent with a THF adduct of $[Rh_2(ap)_4(C{\equiv}CC_5H_{11})]^+$. The presence of THF is expected, since this solvent was used in the synthesis and purification of $Rh_2(ap)_4(R)$. The molecular ion peak at m/e = 613, which is common to both mass spectra, also appears to

Table II. Selected Atomic Coordinates (×10^4) and Equivalent Isotropic Displacement Parameters (10^3 Å^2)[a]

atom	x	y	z	U(eq)	atom	x	y	z	U(eq)
Rh(1)	1659 (1)	1158 (1)	1790 (1)	33 (1)	Rh(2)	1470 (1)	2679 (1)	2681 (1)	34 (1)
N(1)	2349 (6)	395 (5)	2964 (5)	35 (3)	N(2)	2753 (7)	1933 (5)	3502 (5)	35 (3)
N(3)	3390 (6)	1486 (5)	1410 (5)	33 (3)	N(4)	2812 (7)	3142 (5)	1838 (5)	36 (3)
N(5)	986 (7)	2066 (5)	707 (5)	36 (3)	N(6)	213 (7)	3270 (5)	1782 (5)	36 (3)
N(7)	−88 (7)	977 (5)	2282 (5)	33 (3)	N(8)	165 (7)	2067 (5)	3457 (5)	34 (3)
C(5)	2900 (8)	912 (7)	3578 (6)	35 (4)	C(16)	3673 (9)	2446 (7)	1452 (6)	38 (4)
C(27)	289 (8)	2963 (7)	893 (6)	37 (4)	C(38)	−475 (9)	1386 (7)	3108 (6)	37 (4)
C(45)	1787 (9)	−111 (8)	1066 (6)	43 (4)	C(46)	1780 (9)	−857 (7)	655 (7)	57 (4)

[a] Equivalent isotropic U defined as one-third of the trace of the orthogonalized U_{ij} tensor.

Table III. Selected Bond Lengths (Å) and Bond Angles (deg)

Bond Lengths			
Rh(1)-Rh(2)	2.439 (1)	Rh(1)-N(1)	2.058 (7)
Rh(1)-N(3)	2.047 (7)	Rh(1)-N(5)	2.041 (7)
Rh(1)-N(7)	2.053 (7)	Rh(1)-C(45)	2.021 (10)
Rh(2)-N(2)	2.017 (7)	Rh(2)-N(4)	2.006 (7)
Rh(2)-N(6)	1.999 (7)	Rh(2)-N(8)	2.007 (7)
N(1)-C(1)	1.350 (10)	N(1)-C(5)	1.354 (10)
N(2)-C(5)	1.352 (10)	N(2)-C(6)	1.411 (10)
N(3)-C(12)	1.351 (10)	N(3)-C(16)	1.358 (10)
N(4)-C(16)	1.365 (10)	N(4)-C(17)	1.425 (10)
N(5)-C(23)	1.355 (10)	N(5)-C(27)	1.373 (10)
N(6)-C(27)	1.364 (10)	N(6)-C(28)	1.416 (10)
N(7)-C(34)	1.351 (10)	N(7)-C(38)	1.366 (10)
N(8)-C(38)	1.341 (10)	N(8)-C(39)	1.410 (10)
C(4)-C(5)	1.418 (11)	C(15)-C(16)	1.415 (12)
C(26)-C(27)	1.402 (11)	C(37)-C(38)	1.413 412)
Bond Angles			
N(1)-Rh(1)-Rh(2)	86.6 (2)	N(3)-Rh(1)-Rh(2)	86.4 (2)
N(3)-Rh(1)-N(1)	89.3 (3)	N(5)-Rh(1)-Rh(2)	86.7 (2)
N(5)-Rh(1)-N(1)	173.3 (3)	N(5)-Rh(1)-N(3)	89.3 (3)
N(7)-Rh(1)-Rh(2)	86.5 (2)	N(7)-Rh(1)-N(1)	89.5 (3)
N(7)-Rh(1)-N(3)	172.8 (3)	N(7)-Rh(1)-N(5)	91.1 (3)
C(45)-Rh(1)-Rh(2)	178.9 (3)	C(45)-Rh(1)-N(1)	93.1 (3)
C(45)-Rh(1)-N(3)	94.7 (3)	C(45)-Rh(1)-N(5)	93.6 (3)
C(45)-Rh(1)-N(7)	92.5 (3)	N(2)-Rh(2)-Rh(1)	86.5 (2)
N(4)-Rh(2)-Rh(1)	86.9 (2)	N(4)-Rh(2)-N(2)	89.5 (3)
N(6)-Rh(2)-Rh(1)	86.7 (2)	N(6)-Rh(2)-N(2)	173.2 (3)
N(6)-Rh(2)-N(4)	90.3 (3)	N(8)-Rh(2)-Rh(1)	86.8 (2)
N(8)-Rh(2)-N(2)	89.2 (3)	N(8)-Rh(2)-N(4)	173.6 (3)
N(8)-Rh(2)-N(6)	90.2 (3)	C(1)-N(1)-Rh(1)	121.6 (6)
C(5)-N(1)-Rh(1)	118.6 (6)	C(5)-N(1)-C(1)	119.7 (8)
C(5)-N(2)-Rh(2)	120.8 (6)	C(6)-N(2)-Rh(2)	119.0 (6)
C(6)-N(2)-C(5)	120.2 (8)	C(12)-N(3)-Rh(1)	120.6 (6)
C(16)-N(3)-Rh(1)	120.0 (6)	C(16)-N(3)-C(12)	119.5 (8)
C(16)-N(4)-Rh(2)	119.7 (6)	C(17)-N(4)-Rh(2)	120.8 (6)
C(17)-N(4)-C(16)	119.0 (8)	C(23)-N(5)-Rh(1)	122.1 (6)
C(27)-N(5)-Rh(1)	118.7 (6)	C(27)-N(5)-C(23)	119.2 (8)
C(27)-N(6)-Rh(2)	119.8 (6)	C(28)-N(6)-Rh(2)	121.9 (5)
C(28)-N(6)-C(27)	118.2 (7)	C(34)-N(7)-Rh(1)	121.9 (6)
C(38)-N(7)-Rh(1)	117.9 (6)	C(38)-N(7)-C(34)	120.0 (8)
C(38)-N(8)-Rh(2)	120.7 (6)	C(39)-N(8)-Rh(2)	119.9 (6)
C(39)-N(8)-C(38)	119.3 (8)	N(2)-C(5)-N(1)	118.6 (8)
N(4)-C(16)-N(3)	117.7 (9)	N(6)-C(27)-N(5)	118.2 (8)
N(8)-C(38)-N(7)			

be a THF adduct of the fragment $[Rh_2(ap)_2]^+$. Mass spectra of other Rh–C-bonded complexes were consistent with formula $Rh_2(ap)_4(R)$.

The formation of the Rh-C≡CR bond in $Rh_2(ap)_4(R)$ is also readily identified by infrared spectroscopy (see Table V). For instance, the $\nu_{C\equiv C}$ stretch frequency for $HC\equiv CC_6H_5$ shifted from 2111 to 2050 cm^{-1} upon formation of $Rh_2(ap)_4(C\equiv CC_6H_5)$. In the case of $Rh_2(ap)_4(C\equiv CH)$, $\nu_{C\equiv C}$ is at 1954 cm^{-1}, as compared to the value of 1977 cm^{-1} for free acetylene. These frequencies are comparable with the values of 2081 and 1935 cm^{-1} observed for $(PMe_3)_4Rh(C\equiv CC_6H_5)$ and $(PMe_3)_4Rh(C\equiv CH)$.[6,7] The IR spectrum of $Rh_2(ap)_4(C\equiv CC_5H_{11})$ shows $\nu_{C\equiv C}$ at 1945 cm^{-1}, while the IR spectrum of $Rh_2(ap)_4(C\equiv CC_4H_8C\equiv CH)$ shows two $\nu_{C\equiv C}$ at 1946 and 2112 cm^{-1}, with the latter being the C≡CH group, which is away from the rhodium nuclei. The IR spectrum of $Rh_2(ap)_4(C\equiv CH)$ and the spectra of $[Rh_2(ap)_4(C\equiv CH)]^+$ and $[Rh_2(ap)_4(C\equiv CH)]^-$ in the $\nu_{C\equiv C}$ region are given in Figure 2.

$Rh_2(ap)_4(R)$ complexes are also characterized by electrochemical methods and ESR and UV–vis spectra. The data obtained are presented in Table V. The electronic absorption spectra of $[Rh_2(ap)_4(C\equiv CH)]^+$, $Rh_2(ap)_4(C\equiv CH)$, and $[Rh_2(ap)_4(C\equiv CH)]^-$ are illustrated in Figure 3. The ESR spectra of $Rh_2(ap)_4(C\equiv CH)$ under an atmosphere of argon, air, and dioxygen are shown in Figure 4. Cyclic voltammograms of $Rh_2(ap)_4Cl$ and $Rh_2(ap)_4(C\equiv CH)$ are illustrated in Figure 5.

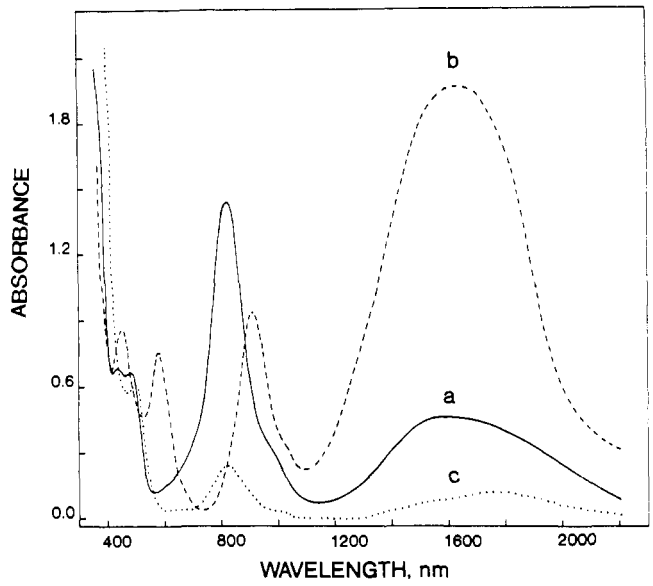

Figure 3. Electronic absorption spectra of 2.4×10^{-4} M $Rh_2(ap)_4(C\equiv CH)$ in CH_2Cl_2 containing 0.1 M TBAP: the neutral (—), singly oxidized (- -), and singly reduced (···) complex.

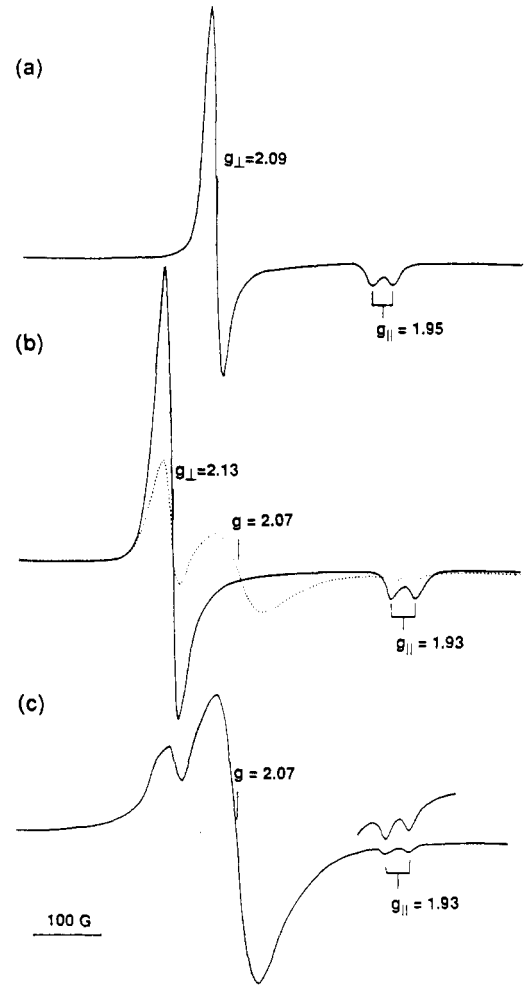

Figure 4. ESR spectra in CH_2Cl_2 at 123 K for (a) 4.0×10^{-4} M $Rh_2(ap)_4Cl$ under Ar, (b) 5.0×10^{-4} M $Rh_2(ap)_4(C\equiv CH)$ under Ar (solid line) and air (dotted line), and (c) $Rh_2(ap)_4(C\equiv CH)$ under 1 atm of O_2. ESR spectra are recorded at a microwave frequency of 9.38 GHz and a field modulation frequency of 100 Hz (modulation intensity 1.25 G_{pp}).

Discussion

Reactivity of $Rh_2(ap)_4Cl$ with Organolithium Reagents. The reaction of $Rh_2(ap)_4Cl$ with lithium alkyls appeared to be restricted

(6) Marder, T. B.; Zargarian, D.; Calabrese, J.; Herskovitz, T. H.; Milstein, D. *J.Chem. Soc. Chem. Commun.* **1987**, 1484.
(7) Zargarian, D.; Chow, P.; Taylor, N. J.; Marder, T. B. *J. Chem. Soc., Chem. Commun.* **1989**, 540.

Table IV. Selected Average Bond Lengths (Å) and Bond Angles (deg) of $Rh_2(ap)_4(L)$ (L = C≡CH or Cl)

	bond length			bond angle	
	L = C≡CH	L = Cl[a]		L = C≡CH	L = Cl[a]
Rh(1)–L	2.021 (1)	2.421 (3)	$Rh(1)–N_p–C$	119.0 (6)	118.5 (3)
Rh(1)–Rh(2)	2.439 (1)	2.406 (1)	$Rh(2)–N_a–C$	120.3 (6)	119.3 (3)
$Rh(2)–N_a$	2.007 (7)	2.009 (4)	$N_a–C–N_p$	118.0 (4)	118.0 (4)
$Rh(1)–N_p$	2.050 (7)	2.049 (3)	N–Rh–Rh–N	22.3	23.4
			Rh(2)–Rh(1)–L	178.9 (3)	180.0
			Rh(1)–C(45)–C(46)	175.6 (9)	

[a] Data taken from ref 2.

Table V. Electronic Absorption Data, Half-Wave Potentials, and ESR Data for Dirhodium Complexes in CH_2Cl_2

				$E_{1/2}$			ESR	
compd	λ ($10^{-3}\epsilon$), nm			2nd ox.	1st ox.	1st red.	$g_\perp$	$g_\parallel$ ($10^4 A_\parallel$, cm^{-1})
$Rh_2(ap)_4(C≡CH)$	475 (2.6)	820 (5.8)	1580 (1.9)	1.03	0.38	−0.63	2.13	1.93 (31.7)
$Rh_2(ap)_4(C≡CC_6H_5)$	510 (2.0)	840 (4.8)	1590 (1.6)	1.09	0.44	−0.62	2.14	1.94 (31.7)
$Rh_2(ap)_4(C≡CC_5H_{11})$	530 (3.0)	845 (5.6)	1590 (1.7)	1.09	0.40	−0.65	2.14	1.93 (32.8)
$Rh_2(ap)_4(C≡CC_4H_8C≡CH)$	535 (2.2)	850 (4.6)	1590 (1.4)	1.03	0.36	−0.67	2.13	1.91 (30.2)
$Rh_2(ap)_4Cl$	495 (3.5)	910 (5.1)	1530 (3.8)		0.52	−0.38	2.09	1.96 (26.4)
$Rh_2(ap)_4ClO_4$	425 (sh)	890 (3.3)	1540 (2.7)		0.53	−0.31	2.08	1.95 (24.5)
$Rh_2(ap)_4(O_2)$	435 (sh)	900 (3.7)	1600 (2.8)			−0.48	2.09	2.03, 1.99[a]

[a] $Rh_2(ap)_4(O_2)$ shows a rhombic signal in CH_2Cl_2.[16]

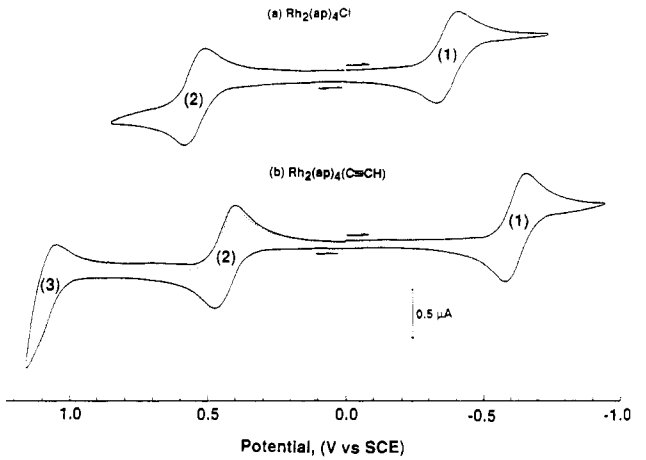

Figure 5. Cyclic voltammograms of 4.5×10^{-4} M (a) $Rh_2(ap)_4Cl$ and (b) $Rh_2(ap)_4(C≡CH)$ in CH_2Cl_2, 0.1 M TBAP, at a scan rate 0.1 V/s.

to compounds that contain terminal acetylenic groups. With these reagents the nucleophilic reaction to form the axial Rh–C bond was rapid at room temperature in dry THF under Ar. No Rh–C-bonded products were isolated from the reaction of $Rh_2(ap)_4Cl$ with saturated alkyllithium compounds, LiC_nH_{2n+1}, for n greater than 1. The formation of $Rh_2(ap)_4(CH_3)$ is observed, but the compound is unstable under the conditions used for purification.

The nucleophilic reactivity is apparently controlled by steric constraints resulting from the hydrogens at position 6 on four pyridyl rings (see Figure 1). These four hydrogens form a cavity about the axial site of rhodium, which limits the binding to small molecules or ions that have near linearity with respect to their lone pair of electrons and the adjacent atom bound to the donor atom, i.e. halide ions, terminal acetylide ions, nitriles, etc. The steric hindrance created by four phenyl groups on anilino nitrogen at the second rhodium atom is much greater. Thus, only monoadducts have appreciable stability, and the first axial ligation always takes place on the pyridyl-bound rhodium in the 4,0 geometric isomer of $[Rh_2(ap)_4]^{n+}$ (n = 0, 1, 2).

Structure of $Rh_2(ap)_4(C≡CH)$. An increased Rh–Rh bond distance from 2.406 Å in $Rh_2(ap)_4Cl$ to 2.439 Å in $Rh_2(ap)_4(C≡CH)$ reflects the strong electron-donor property of $C≡CH^-$ (see Table IV). Very few structural differences exist between these two complexes with respect to the equatorial Rh–N bonds. For example, the average $Rh(2)–N_a$ (anilino) and $Rh(1)–N_p$ (pyridyl) bond lengths of 2.007 and 2.050 Å in $Rh_2(ap)_4(C≡CH)$ are essentially the same as those of the chloride complex. The average $Rh(1)–N_p–C$, $Rh(2)–N_a–C$, and $N_a–C–N_p$ bond angles also show little change between the two compounds. The average N–Rh–Rh–N torsional angle decreases slightly from 23.4° in $Rh_2(ap)_4Cl$ to 22.3° in $Rh_2(ap)_4(C≡CH)$.

The $Rh–N_a$ bond distance is 0.043 Å shorter than the $Rh–N_p$ distance in $Rh_2(ap)_4(C≡CH)$. This could result from a greater concentration of negative charge on the anilino nitrogens and/or a larger effective nuclear charge on the anilino nitrogen bound rhodium ion. The fact that the average $Rh–N_a$ and $Rh–N_p$ bond distances for the 2,2-trans isomer of $Rh_2(ap)_4(NCC_6H_5)$ are almost the same[2] and very close in value to the $Rh–N_p$ bond distance of $Rh_2(ap)_4(C≡CH)$ suggests that N_a bound rhodium of the latter complex has a higher effective nuclear charge (less d-electron shielding along Rh–N-bond axes) than N_p bound rhodium. This probably is the major factor for the shorter $Rh–N_a$ bond distance.

The Rh–C bond distance of 2.021 Å observed for $Rh_2(ap)_4(C≡CH)$ is comparable with the bond lengths of 2.035, 2.02, and 2.002 Å reported for mononuclear rhodium complexes $[(PMe_3)_4Rh(H)(C≡CCH_2CH_2OH)]Cl$, $(PMe_3)_4Rh(C≡CSiMe_3)$, and $(PMe_3)_4Rh(C≡CC_6H_5)$.[6,7] In these examples, the first complex contains a Rh^{III}, while the last two contain Rh^{I}.

UV–Vis Spectra of $[Rh_2(ap)_4(R)]^{+,0,-}$. Neutral $Rh_2(ap)_4(C≡CH)$ shows two closely spaced absorptions at 440 (sh) and 475 nm ($\epsilon = 2.6 \times 10^3$), a strong band at 820 nm ($\epsilon = 5.8 \times 10^3$), and a near-infrared band at 1580 nm ($\epsilon = 1.9 \times 10^3$) (curve a, Figure 3), while its parent complex $Rh_2(ap)_4Cl$ has absorptions at 495 ($\epsilon = 3.5 \times 10^3$), 910 ($\epsilon = 5.1 \times 10^3$), and 1530 nm ($\epsilon = 3.8 \times 10^3$).[2] The singly oxidized complex, $[Rh_2(ap)_4(C≡CH)]^+$, displays absorptions at 450 ($\epsilon = 4.1 \times 10^3$), 580 ($\epsilon = 3.7 \times 10^3$), 910 ($\epsilon = 4.4 \times 10^3$), and 1650 nm ($\epsilon = 8.6 \times 10^3$) (curve b, Figure 3). Singly reduced $Rh_2(ap)_4(C≡CH)$ shows only a shoulder at 500 nm (curve c, Figure 3). The weak peak at 820 nm and the broad absorbance between 1250 and 2100 nm observed in curve c are due to unreduced $Rh_2(ap)_4(C≡CH)$.

$Rh^{II}Rh^{III}$ complexes generally have three strong absorption peaks in the visible and near-IR region of the spectra. As seen in Table V, the higher energy visible band shows the largest variation, ranging from 425 nm for the nonbonding perchlorate to 535 nm for $Rh_2(ap)_4(C≡CC_4H_8C≡CH)$. The lower energy visible band and near-IR band are relatively insensitive to the σ-donor ability of the axial anion.

Theoretical calculations reported for $Rh_2(HNCHNH)_4$, which has eight nitrogen donor atoms similar to the (anilinopyridinato)dirhodium complexes,[8,9] suggest the existence of a single

(8) Rizzi, G. A.; Casarin, M.; Tondello, E.; Piraino, P.; Granozzi, G. *Inorg. Chem.* **1987**, *26*, 3406.
(9) Cotton, F. A.; Feng, X. *Inorg. Chem.* **1989**, *28*, 1180.

σ bond corresponding to the electronic configuration of $\sigma^2\pi^4\delta^2\pi^{*4}\delta^{*2}$. The antibonding orbitals are closely spaced and similar in energy to two of the nitrogen π combinations. For the formamidinate complex the HOMO is found to be the $\delta^*_{Rh-Rh}\pi^*_{Rh-N}$ orbital with a high-percent population density on amidinate nitrogens. The available information on this complex system is not sufficient for a detailed assignment of the origin of UV–vis and near-IR absorbance peaks for $Rh_2(ap)_4(R)$. However, there are several features observed in the spectra of these complexes that can be addressed. The near-IR and lower energy visible bands are only present when dirhodium complexes are in formal oxidation states of $Rh^{II}Rh^{III}$ or Rh^{III}_2. This suggests that these transitions involve the excitation of an electron from a lower lying orbital to the δ^*_{Rh-Rh} orbital (SOMO for $Rh^{II}Rh^{III}$ and LUMO for Rh^{III}_2). The intensity of the peaks indicates that these transitions are charge transfer in nature and could involve ligand to metal charge-transfer processes (N π combinations to metal δ^*_{Rh-Rh}) and/or intervalent metal to metal charge-transfer transitions. The latter possibility results from δ^*_{Rh-Rh} being localized on one rhodium ion.

ESR Spectra. ESR studies of the 4,0 geometric isomer of $Rh_2(ap)_4Cl$ have shown that the SOMO is localized on one rhodium, giving a true mixed-valent $Rh^{II}Rh^{III}$ complex.[1,2] This complex gives the axially symmetric signal in frozen CH_2Cl_2 solution, as shown in Figure 4a with $g_\parallel$ split into a doublet ($A_\parallel = 26.4 \times 10^{-4}$ cm^{-1}). Similar ESR spectra are observed when the axially coordinated chloride ion is replaced by acetylide ions. For example, the ESR spectrum of $Rh_2(ap)_4(C{\equiv}CH)$ in CH_2Cl_2 under Ar shows a signal with $g_\perp = 2.13$ and $g_\parallel = 1.93$ with $A_\parallel = 31.7 \times 10^{-4}$ cm^{-1} (solid line, Figure 4b).

No ESR spectrum is observed for frozen solutions of $[Rh_2(ap)_4(L)]^+$ or $[Rh_2(ap)_4(L)]^-$ generated by electrochemical oxidation or reduction. There is no question that $[Rh_2(ap)_4(L)]^-$ should be diamagnetic. However $[Rh_2(ap)_4(L)]^+$ is isoelectronic with tetrabridged Ru^{II}_2 complexes, which are paramagnetic when the bridging ligands are $RCOO^-$ ions[10] and diamagnetic when bridging ligands are (*p*-tolyl)NNN(*p*-tolyl) ions.[11] Theoretical calculations[9] on the latter complex show that $E(\delta^*_{Ru-Ru}) \gg E(\pi^*_{Ru-Ru})$. Under these conditions $Ru_2(tol)_4$ would have the electronic configuration $\sigma^2\pi^4\delta^2\pi^{*4}$ and be diamagnetic, which is consistent with experimental results.[10,11] The δ^*_{Rh-Rh} for $[Rh_2(ap)_4(L)]^+$ should also be highly stabilized through interaction with the bridging ligand's NCN nonbonding π combinations, resulting in a diamagnetic complex like $Ru_2(tol)_4$.

Theoretical and experimental studies of g tensors of Rh_2^{5+} complexes predict a $g_\parallel < g_e$ when the SOMO is δ^*_{Rh-Rh} and a $g_\parallel > g_e$ when it is σ_{Rh-Rh} or π^*_{Rh-Rh}.[12,13] Therefore, the g tensor for $Rh_2(ap)_4Cl$ is consistent with a δ^*_{Rh-Rh} SOMO. Calculations on $Rh_2(HNCHNH)_4$ also give a δ^*_{Rh-Rh} HOMO.[8,9] If the nature of the SOMO of $Rh_2(ap)_4Cl$ remains the same upon substitution of chloride by other anions, then the difference between $g_\perp$ and $g_\parallel$ and the value of $A_\parallel$ should reflect differences in the axial and equatorial ligand fields induced by the axial ligation. This appears to be the case, as both $Rh_2(ap)_4(C{\equiv}CH)$ and $Rh_2(ap)_4Cl$ give axial signals with $g_\parallel < g_e$. In addition, the difference between $g_\perp$ and $g_\parallel$ and the value of $A_\parallel$ both increase with an increasing donor ability of the axial anion (Table V). Only small variations are observed in *g* and *A* values among the acetylide complexes.

Another important result is that $g_\parallel$ is a 1:1 doublet for the complex with the perchlorate counterion. If ClO_4^- is a nonbonding anion in CH_2Cl_2, then the localization of the unpaired electron in $Rh_2(ap)_4(ClO_4)$ is primarily due to the different equatorial ligand fields of the two rhodium ions and/or the decoupling of the d_{xy}–d_{xy} interaction by the twist of two equatorial rhodium planes.

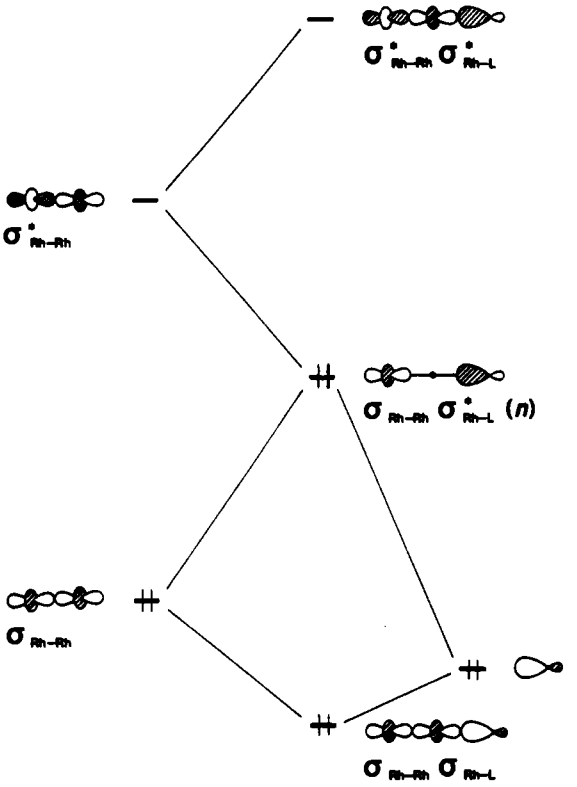

Figure 6. σ molecular orbital pattern for axial binding of the dirhodium complex.

It is clear that the SOMO for the 4,0 isomer of $[Rh_2(ap)_4]^+$ is localized on one rhodium, and there is strong evidence that it is the δ^*_{Rh-Rh} orbital. However, there are questions regarding the direction of polarization of the SOMO of $[Rh_2(ap)_4]^+$ and $Rh_2(ap)_4(R)$. The only theoretical calculation that specifically addresses this question was reported recently on the 4,0 geometric isomers of $[Rh_2(tcl)_4CO]^+$ (tcl = ω-thiocaprolactamate).[14] The results suggested that if localization of the SOMO occurred, the odd electron would be on $Rh(S)_4$ for the former complex and on $Rh(N)_4$ for the latter. ESR spectra of $[Rh_2(tcl)_4(tclH)]^+$, however, showed an axial signal with $g_\perp$ at 2.11 and a broad signal for $g_\parallel$ at 2.02 with no observable hyperfine splitting. Therefore ESR results were more consistent with a σ_{Rh-Rh} SOMO.[12,13] Because of the presence of S donors in $[Rh_2(tcl)_4]^+$, this complex does not provide a good comparison with $[Rh_2(ap)_4]^+$.

Anilino nitrogens in ap bridging ligands are stronger σ and π donors than pyridyl nitrogens. The twist of two rhodium planes by ~23° will also substantially decrease the d_{xy}–d_{xy} overlap and tend to localize each of the d_{xy} orbitals on their respective rhodium centers. Therefore the energy of the d_{xy} orbital of the anilino nitrogen bound rhodium should have the highest energy and be the HOMO of the neutral unligated complex, $Rh_2(ap)_4$, and the SOMO of its singly oxidized state.

Axial ligation to the pyridyl nitrogen bound rhodium will primarily affect the Rh–Rh MO's with σ symmetry. The axial ligand's donor function will interact with the σ_{Rh-Rh} and σ^*_{Rh-Rh} orbitals to form a classical three-orbital problem,[2,15] as shown in Figure 6. Extended Huckel calculations on the model compound, $Rh_2(HNCHNH)_4L$, show[2] that the lowest energy MO is localized on the axial ligand with σ_{Rh-Rh} mixed in a bonding fashion. The middle level, *n*, is predominantly σ_{Rh-Rh} destabilized by the axial ligand. σ^*_{Rh-Rh} mixes into this orbital in a bonding fashion to the axial donor function and decreases the amplitude on the axially coordinated rhodium. The highest energy MO is primarily σ^*_{Rh-Rh} with the axial donor function mixed into it in an antibonding fashion. The energy and degree of polarization of *n* toward the

(10) Lindsay, A. J.; Wilkinson, G.; Motevalli, M.; Hursthouse, M. B. *J. Chem. Soc., Dalton Trans.* **1985**, 2321.
(11) Cotton, F. A.; Matusz, M. *J. Am. Chem. Soc.* **1988**, *110*, 5761.
(12) Kawamura, T.; Katayama, H.; Yamabe, T. *Chem. Phys. Lett.* **1986**, *130*, 20.
(13) Kawamura, T.; Fukamachi, K.; Sowa, T.; Hayashida, S.; Yonezawa, T. *J. Am. Chem. Soc.* **1981**, *103*, 364.
(14) Poblet, J. M.; Benard, M. *Inorg. Chem.* **1988**, *27*, 2935.
(15) Albright, T. A.; Burdett, J. K.; Whangbo, M. H. *Orbital Interaction in Chemistry*; Wiley: New York, 1985.

axially uncoordinated rhodium ion depend on the strength of the axial σ donor (amount of σ^*_{Rh-Rh} mixed into the MO). In the extreme case where n is highly polarized toward $Rh(N_a)_4$, the odd electron is still localized in $\delta^*(d_{xy})$ for $(N_a)_4RhRh(N_p)_4(L)$ and remains on $Rh(N_a)_4$.

Coordination of Dioxygen by $Rh_2(ap)_4(R)$. We have previously reported that the 4,0 isomer of $Rh^{II}_2(ap)_4$ reacts rapidly with dioxygen to form a stable superoxide complex, where oxygen was ligated on the rhodium atom with four pyridyl nitrogens.[16] There is now evidence that $Rh^{II}Rh^{III}(ap)_4(R)$ complexes also form dioxygen complexes. For example, both $g_\perp$ and $g_\parallel$ decrease in intensity and a new broad signal is observed at $g = 2.07$ when the ESR spectrum of $Rh_2(ap)_4(C{\equiv}CH)$ was measured in frozen CH_2Cl_2 saturated with dry air (dotted line, Figure 4b). This signal indicates the formation of $Rh_2(ap)_4(C{\equiv}CH)(O_2)$, where O_2 is bound to the rhodium ion with four anilino nitrogens, as the other rhodium atom is already bonded with the acetylide ion:

$$Rh_2(ap)_4(C{\equiv}CH) + O_2 \leftrightarrow Rh_2(ap)_4(C{\equiv}CH)(O_2) \quad (1)$$

Upon bubbling pure O_2 through the solution, the signal at $g = 2.07$ becomes much larger while the original signal at $g = 2.13$ continues to decrease (Figure 4c). In addition, a shoulder on the signal at $g = 2.13$ appears. The $Rh_2(ap)_4(C{\equiv}CH)$ spectrum reappears when the O_2 atmosphere is replaced by Ar or when CH_3CN is added to the CH_2Cl_2 solution. Therefore the acetylide ion remains bound to rhodium upon the association and dissociation of dioxygen, as shown in reaction 1. Acetonitrile apparently competes for the available axial site with dioxygen and forms $Rh_2(ap)_4(C{\equiv}CH)(CH_3CN)$ ($g_\perp = 2.14$, $g_\parallel = 1.93$, and $A_\parallel = 30.4 \times 10^{-4}$ cm^{-1}). The ESR data suggest that small linear ligands such as O_2 and CH_3CN can bind to the axial site of the $Rh(N_a)_4$ unit. Dioxygen complex formation was also observed to some degree for $Rh_2(ap)_4Cl$, $Rh_2(ap)_4(ClO_4)$, and all other acetylide complexes in frozen CH_2Cl_2.

ESR spectra of $Rh_2(ap)_4(R)(O_2)$ are similar to those observed for dioxygen adducts of cobalt(II) complexes such as $Co^{II}TPP(CO)(O_2)$ ($g_\parallel = 2.070$, $g_\perp = 2.014$; TPP = tetraphenylporphyrinato dianion)[17] and $Co^{II}(TPP)(DMSO)(O_2)$ ($g_\parallel = 2.089$, $g_\perp = 1.998$).[18] The spin-pairing model of binding dioxygen to a low-spin Co^{II} may be extended to the bonding in the dirhodium complexes. Since rhodium hyperfine splitting is not observed in the ESR spectra of $Rh_2(ap)_4(R)(O_2)$, the extent of electron transfer to dioxygen could be quite large.

The above results show that bis axial adducts can be formed through the oxidative coordination of dioxygen with $Rh_2(ap)_4(R)$. The reactivity at the second rhodium site is controlled by the steric constraint formed by four phenyl groups and the σ-donor ability of the axial ligand bound to $Rh(N_p)_4$. The latter effect results from polarization of n (Figure 4), which places more electron density on $Rh(N_a)_4$. The net result is an increase in the energy of the SOMO and a cathodic shift in the $Rh^{II}Rh^{III}/Rh^{III}_2$ redox potential. Dioxygen binding should also be enhanced by lowering the temperature to reduce the rotation of nitrogen phenyl groups.

No band corresponding to bound O_2^- was observed in the IR spectrum of $Rh_2(ap)_4(C{\equiv}CH)(O_2)$. The complex has several strong bands in the region where the O–O$^-$ stretch should appear, and this band could be quite weak and unresolved. There is a slight shift of ν_{CCH} in the solid-state infrared spectrum (Figure 2) of the complex obtained by evaporation of a CH_2Cl_2 solution containing $Rh_2(ap)_4(C{\equiv}CH)$ under O_2. However, solution spectra of $Rh_2(ap)_4(C{\equiv}CH)$ in CH_2Cl_2 taken under N_2 or O_2 both showed the same $\nu_{C{\equiv}C}$ band at 1954 cm^{-1}. A further indication of the absence of O_2 bonding or of weak O_2 bonding in solution at room temperature is shown by the same half-wave potentials of $Rh_2(ap)_4(R)$ in CH_2Cl_2 under N_2 or O_2. Therefore, O_2 binding may only occur at the cold temperature of the ESR measurement.

Electrochemistry. $Rh_2(ap)_4Cl$ displays one reduction and one oxidation wave ($E_{1/2} = -0.38$ and 0.52 V vs SCE) in CH_2Cl_2, 0.1 M TBAP.[2] These waves correspond to the $Rh^{II}_2/Rh^{II}Rh^{III}$ and $Rh^{II}Rh^{III}/Rh^{III}_2$ redox couples. The formation of $Rh_2(ap)_4(C{\equiv}CH)$ from the chloride complex shifts $E_{1/2}$ of the first reduction from −0.38 to −0.63 V and $E_{1/2}$ of the first oxidation from 0.52 to 0.38 V (Figure 5). $Rh_2(ap)_4(C{\equiv}CH)$ also shows a new oxidation wave at $E_{1/2} = 1.03$ V (wave 3, Figure 5b). The reactions can be represented as eqs 2–4. All other $Rh_2(ap)_4(R)$ complexes

$$Rh_2(ap)_4(C{\equiv}CH) + e^- \leftrightarrow [Rh_2(ap)_4(C{\equiv}CH)]^- \quad (2)$$

$$Rh_2(ap)_4(C{\equiv}CH) \leftrightarrow [Rh_2(ap)_4(C{\equiv}CH)]^+ + e^- \quad (3)$$

$$[Rh_2(ap)_4(C{\equiv}CH)]^+ \leftrightarrow [Rh_2(ap)_4(C{\equiv}CH)]^{2+} + e^- \quad (4a)$$

$$\rightarrow \text{chem reactions} \quad (4b)$$

give cyclic voltammograms similar to that of $Rh_2(ap)_4(C{\equiv}CH)$ (Table V). Very little variation is observed in redox potentials among different acetylide adducts. Since the HOMO and SOMO of the 4,0 isomer are localized on the rhodium ion bound to four stronger σ- and π-donor anilino nitrogens, the cathodically shifted redox potentials reflect the increase in electron density on $Rh(N_a)_4$ upon axial ligation at the pyridyl-bound rhodium. The magnitude of the shift is related to the degree of axial polarization of the $\sigma_{Rh-Rh}\sigma^*_{Rh-L}$ orbital.

Even though the peak heights of all three cyclic waves indicate an equal number of electrons being transferred for each process, controlled-potential electrolyses reveal that 1.0 ± 0.1, 0.9 ± 0.1, and 3.7 ± 0.5 electrons are transferred for reactions 2–4. Apparently, the product of reaction 4a is only stable on the cyclic voltammetric time scale and some type of chemical reactions occur after the electron transfer (eq 4b). It is not clear whether reaction 4a involves a metal- or ligand-centered oxidation. A transient product could not be trapped for ESR measurements because the rhodium-containing species accumulates on the electrode surface during electrolysis. Since four electrons are involved in overall reactions 4a,b, some or all equatorial ligands are probably oxidized.

As discussed earlier, $\nu_{C{\equiv}C}$ for $HC{\equiv}CH$ shifted from 1977 to 1954 cm^{-1} upon formation of $Rh_2(ap)_4(C{\equiv}CH)$. An infrared spectroelectrochemical technique[19] was used to characterize $Rh_2(ap)_4(C{\equiv}CH)$ in its singly reduced, singly oxidized, and doubly oxidized states. Insets a and b of Figure 2 (solid line) show the IR spectrum of $Rh_2(ap)_4(C{\equiv}CH)$ in CH_2Cl_2, 0.1 M TBAP, between 2000 and 1900 cm^{-1}. When the complex is reduced at −0.8 V to $[Rh_2(ap)_4(C{\equiv}CH)]^-$, a new peak is found at 1922 cm^{-1} (dashed line in inset a, Figure 2). When the complex is oxidized at 0.8 V to $[Rh_2(ap)_4(C{\equiv}CH)]^+$, $\nu_{C{\equiv}C}$ is found at 1972 cm^{-1} (dashed line in set b, Figure 2). The product of the doubly oxidized $[Rh_2(ap)_4(C{\equiv}CH)]$ precipitates from CH_2Cl_2 solution as a black material. The IR spectrum of the precipitate shows only very weak bands corresponding to the bridging ligands, which indicates that most bridging ligands remain in solution after decomposition.

IR data of a series of Rh^{III} and Rh^I σ-acetylide complexes have been recently reported. $\nu_{C{\equiv}C}$ for the complexes $[(PMe_3)_4Rh^{III}(C{\equiv}CC_6H_5)(H)]Cl$, $(PMe_3)_4Rh^I(C{\equiv}CC_6H_5)$, and $(PMe_3)_4Rh^I(C{\equiv}CH)$ was found at 2110, 2081, and 1935 cm^{-1}, respectively.[6,7] The acetylide ion is a strong σ-donor ligand that can also accept rhodium π-electron density into its two empty π^* orbitals. The decrease in $\nu_{C{\equiv}C}$ from 2110 cm^{-1} for the cationic d^6 complex to 2081 cm^{-1} for the neutral d^8 complex was attributed to weak π-acceptor behavior of the acetylide ion.[7] Therefore, the larger $\Delta\nu_{C{\equiv}C}$ observed between $[Rh_2(ap)_4(C{\equiv}CH)]^+$ ($\nu_{C{\equiv}C}$ = 1972 cm^{-1}) and $[Rh_2(ap)_4(C{\equiv}CH)]^-$ ($\nu_{C{\equiv}C}$ = 1922 cm^{-1}) suggests some mixing of the π^*_{Rh-Rh} with the acetylide π^* molecular orbitals for the Rh^{II}_2 complex.

In summary, $Rh_2(ap)_4(R)$ can be prepared by direct reaction of $Rh_2(ap)_4Cl$ with LiR. Stable Rh–C bond formation is restricted to terminal acetylide ions because of steric hindrance (pyridyl hydrogens) about the axial site. The coordination of the dirhodium

(16) Bear, J. L.; Yao, C.-L.; Capdevielle, F. J.; Kadish, K. M. *Inorg. Chem.* **1988**, *27*, 3782.
(17) Wayland, B. B.; Minkiewiez, J. V.; Abd-Elmazeed, M. E. *J. Am. Chem. Soc.* **1974**, *96*, 2795.
(18) Ozawa, T.; Hanaki, A. *Inorg. Chim. Acta* **1988**, *153*, 201.
(19) Yao, C.-L.; Capdevielle, F. J.; Kadish, K. M.; Bear, J. L. *Anal. Chem.* **1989**, *61*, 2805.

unit by strong σ-donor alkyl ions significantly increases the electron density on rhodium centers and causes a large cathodic shift of redox potentials. ESR results show that the localization of the SOMO of $[(N_a)_4RhRh(N_p)_4]^+$ complexes on the $(N_a)_4Rh$ center is due to differences in equatorial bonding environments and twisting of two rhodium planes. Additional polarization of electron density on the two metal centers is related to the σ-donor strength of the axial anion. These complexes can undergo oxidative coordination with O_2 to form $Rh_2(ap)_4(R)(O_2)$ with a formal Rh^{III}_2 unit. This and previously reported results[16] show dioxygen complexes of the $Rh_2(ap)_4$ unit with Rh^{II}_2, $Rh^{II}Rh^{III}$, and Rh^{III}_2 formal oxidation states. The degree of O_2 activation decreases in the order of $[Rh_2(ap)_4(O_2)]^- > Rh_2(ap)_4(O_2) > [Rh_2(ap)_4(O_2)]^+ > Rh_2(ap)_4(C{\equiv}CH)(O_2)$ and ranges from the highly reactive superoxide ion in $[Rh_2(ap)_4(O_2)]^-$ to the weakly reversibly bound dioxygen in $Rh_2(ap)_4(C{\equiv}CH)(O_2)$.

Acknowledgment. We thank the Robert A. Welch Foundation for generous support through Grant No. E-918, and K.H.P. and M.-J.J. thank the Korea Minister of Education for support of the visiting scholarship.

Supplementary Material Available: Tables S1–S3, listing data collection and processing parameters, anisotropic thermal parameters, and hydrogen atomic coordinates, Figure S4, showing the mass spectra of (a) $Rh_2(ap)_4(C{\equiv}CC_6H_5)$ and (b) $Rh_2(ap)_4(C{\equiv}CC_5H_{11})$, Figure S5, containing the molecular packing diagram of $Rh_2(ap)_4(C{\equiv}CH)\cdot CH_2Cl_2$, and Table S6, listing atomic coordinates (7 pages); Table S7, listing observed and calculated structure factors (13 pages). Ordering information is given on any current masthead page.

Contribution from the Department of Chemistry,
The University of Alberta, Edmonton, Alberta, Canada T6G 2G2

Oxidative-Addition Reactions Involving the Mixed-Valence Complex $[RhRe(CO)_4(Ph_2PCH_2PPh_2)_2]$. Influence of the Coordinatively Unsaturated Rh(+I) Center on the Saturated Re(−I) Center

David M. Antonelli and Martin Cowie*

Received February 12, 1990

The mixed-metal complex $[RhRe(CO)_4(dppm)_2]$ (**1**) (dppm = $Ph_2PCH_2PPh_2$) undergoes facile oxidative-addition reactions with H_2, Cl_2, and HCl and also reacts with $HBF_4\cdot Et_2O$ and with the activated alkynes, dimethyl acetylenedicarboxylate (DMA), and hexafluoro-2-butyne (HFB). In the protonation reaction and the alkyne reactions these groups bridge the metals with retention of all carbonyl groups. In the reactions with H_2, Cl_2, and HCl both atoms of the attacking substrate bridge the metals on opposite sides of the $RhReP_4$ plane, and loss of one carbonyl group from Re occurs. Loss of one carbonyl from Re can also occur for the alkyne complexes, and this is accompanied by donation of a pair of electrons from Rh. The structure of the protonated complex $[RhRe(CO)_4(\mu\text{-}H)(dppm)_2][BF_4]\cdot H_2O$ (**2**) has been determined crystallographically. This compound crystallizes in the monoclinic space group $P2_1/n$ with a = 17.257 (3) Å, b = 12.235 (2) Å, c = 26.354 (3) Å, β = 102.31 (1)°, V = 5436 (3) Å^3, and Z = 4. On the basis of 5535 unique observations and 388 parameters varied, the structure has refined to R = 0.043 and R_w = 0.060. Protonation at the Rh–Re bond has resulted in a lengthening of this separation from 2.7919 (6) to 3.0036 (7) Å, and a rearrangement of the carbonyl groups on Re, from a trigonal arrangement in **1** to an arrangement in which they occupy three meridional sites of an octahedron in **2**.

Introduction

Oxidative-addition reactions are of fundamental importance in organometallic chemistry[1,2] and offer additional challenges in polynuclear complexes owing to the possible involvement of the adjacent metals.[3-6] As part of an investigation into the reactivity of low-valent diphosphine-bridged heterobinuclear complexes,[7-10] we have undertaken a study of the oxidative addition and related reactions involving the mixed-metal species $[RhRe(CO)_4(dppm)_2]$ (**1**). The structural characterization of this species led to its formulation as a mixed-valence complex in which a donor–acceptor bond links the coordinatively unsaturated Rh(+I) center and the saturated Re(−I) center.[11] Whether compound **1** is formulated

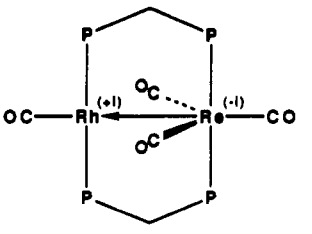

1

as a Rh(I)/Re(−I) species, as suggested, or as a more conventional Rh(0)/Re(0) species, it was felt that the low oxidation states of the metals and the coordinative unsaturation at Rh should make the complex prone to oxidative addition reactions. It was of interest to establish the influence of each metal on the other and, in particular, to establish whether the coordinatively unsaturated Rh(+I) center would increase the reactivity of the otherwise inert $Re(CO)_3P_2^-$ moiety. The related dirhenium complex $[Re_2(CO)_6(dppm)_2]$, in which *both* metals are coordinatively saturated,

(1) Collman, J. P.; Hegedus, L. S.; Norton, J. R.; Finke, R. G. *Principles and Applications of Organotransition Metal Chemistry*; University Science Books: Mill Valley, CA, 1987; p 279.
(2) Collman, J. P.; Roper, W. R. *Adv. Organomet. Chem.* **1968**, *7*, 53.
(3) Halpern, J. *Inorg. Chim. Acta* **1982**, *62*, 31.
(4) Trinquier, G.; Hoffmann, R. *Organometallics* **1984**, *3*, 370.
(5) Schenck, T. G.; Milne, C. R. C.; Sawyer, J. F.; Bosnich, B. *Inorg. Chem.* **1985**, *24*, 2338.
(6) Atwood, J. L.; Beveridge, K. A.; Bushnell, G. W.; Dixon, K. R.; Eadie, D. T.; Stobart, S. R.; Zaworotko, M. J. *Inorg. Chem.* **1984**, *23*, 4050.
(7) Vaarstra, B. A.; Cowie, M. *Inorg. Chem.* **1989**, *28*, 3138.
(8) Vaartstra, B. A.; Cowie, M. *Organometallics* **1989**, *8*, 2388.
(9) Antonelli, D. M.; Cowie, M. *Inorg. Chem.* **1990**, *29*, 3339.
(10) McDonald, R.; Cowie, M. Manuscript in preparation.
(11) Antonelli, D. M.; Cowie, M. *Organometallics* **1990**, *9*, 1818.

0020-1669/90/1329-4039$02.50/0